

Porphyrin-Derived Graphene-Based Nanosheets Enabling Strong Polysulfide Chemisorption and Rapid Kinetics in Lithium–Sulfur Batteries

Long Kong, Bo-Quan Li, Hong-Jie Peng, Rui Zhang, Jin Xie, Jia-Qi Huang, and Qiang Zhang*

Lithium–sulfur (Li–S) batteries hold great promise as a next-generation battery system because of their extremely high theoretical energy density and low cost. However, ready lithium polysulfide (LiPS) diffusion and sluggish redox kinetics hamper their cyclability and rate capability. Herein, porphyrin-derived graphene-based nanosheets (PNG) are proposed for Li–S batteries, which are achieved by pyrolyzing a conformal and thin layer of 2D porphyrin organic framework on graphene to form carbon nanosheets with a spatially engineered nitrogen-dopant-enriched skin and a highly conductive skeleton. The atomic skin is decorated with fully exposed lithiophilic sites to afford strong chemisorption to LiPSs and improve electrolyte wettability, while graphene substrate provides speedy electron transport to facilitate redox kinetics of sulfur species. The use of PNG as a lightweight interlayer enables efficient operation of Li–S batteries in terms of superb cycle stability (cyclic decay rate of 0.099% during 300 cycles at 0.5 C), good rate capability (988 mAh g⁻¹ at 2.0 C), and impressive sulfur loading (areal capacity of 8.81 mAh cm⁻² at a sulfur loading of 8.9 mg cm⁻²). The distinct interfacial strategy is expected to apply to other conversion reaction batteries relying on dissolution–precipitation mechanisms and requiring interfacial charge- and mass-transport-mediation concurrently.

energy density of 2600 Wh kg⁻¹, which vastly exceeds that of the state-of-the-art lithium-ion batteries.^[2] The sulfur cathode undergoes a series of reduction reactions during the complex Li–S electrochemistry, generating soluble lithium polysulfides (LiPSs) with various chain lengths and insoluble lithium disulfide/sulfide (Li₂S₂/Li₂S) in sequence. A theoretical capacity of 1675 mAh g⁻¹ can be thereby deduced assuming the fully lithiation of sulfur to Li₂S.^[3,4] These conversion reactions of sulfur relying on a dissolution–precipitation mechanism, together with inherently poor electrical/ionic conductivities of intermediate- and end-products (sulfur, LiPSs, and Li₂S/Li₂S), pose grand challenges to achieve reliable Li–S batteries.^[5,6] The intermediate LiPSs infinitely circulate between electrodes and react with lithium anode, causing gradual sulfur loss and low Coulombic efficiency. Besides, the insulating solid products necessitate a large portion of conductive agents, offsetting the key advantage of energy-dense Li–S batteries.^[7] Therefore, immobilizing LiPSs

The rising demand for mobile applications and grid-scale energy storage has motivated the development of battery technologies outperforming current lithium-ion batteries in terms of energy/power densities, safety, and material sustainability.^[1] Lithium–sulfur (Li–S) batteries gain momentum among potential battery systems owing to the appealing theoretical

and propelling redox kinetics of sulfur species are key to advancing Li–S batteries,^[3,8] especially in the case where critical parameters such as high sulfur loading, high sulfur content, and low electrolyte dosage are required in more practical battery protocols.^[9]

Carbonaceous materials have been widely applied as sulfur hosts to enhance the conductivity of sulfur composite cathodes and sterically block the diffusion of LiPSs.^[10] However, non-polar nanocarbon materials always exhibit poor affinity to LiPSs and undesirable wetting properties for smooth electrolyte infiltration and rapid lithium-ion transfer.^[11,12] Heteroatom dopants in carbon scaffolds have been experimentally and theoretically demonstrated to anchor LiPSs within cathode side due to the formation of lithium bonds.^[13,14] However, heavily doped heteroatoms across the bulk materials might introduce considerable defects and ruin the ideally delocalized electron-transporting system,^[15] thus reducing the bulk electrical conductivity. Such an undesirable reduction in electrical conductivity is against to offering fast kinetics of sulfur conversion reactions. Other functional materials, such as metal oxides,^[16,17] metal sulfides,^[18,19] metal nitrides,^[20–22] metal phosphates,^[23] and

Dr. L. Kong, B.-Q. Li, H.-J. Peng, R. Zhang, J. Xie, Prof. Q. Zhang
Beijing Key Laboratory of Green Chemical Reaction Engineering and Technology
Department of Chemical Engineering
Tsinghua University
Beijing 100084, China
E-mail: zhang-qiang@mails.tsinghua.edu.cn

Prof. J.-Q. Huang
Advanced Research Institute of Multidisciplinary Science
Beijing Institute of Technology
Beijing 100081, China

 The ORCID identification number(s) for the author(s) of this article can be found under <https://doi.org/10.1002/aenm.201800849>.

DOI: 10.1002/aenm.201800849

polymers,^[24] embedded in conductive matrix are also proved to suppress LiPS shuttling by exerting Lewis acid–base interaction,^[22,25] strong chemical bonding,^[17,26] and/or favorable catalytic effects.^[18,27] Nevertheless, these materials are limited by either only partially exposing adsorptive sites or providing a moderate electrical conductivity.^[28] It is very challenging to meet the demands for superb specific chemisorption to LiPSs (with respect to the mass of sulfur host) and high electrical conductivity simultaneously through a single material.^[29]

In this contribution, porphyrin-derived graphene-based nanosheets (PNG) are synthesized by directly growing a conformal and thin layer of 2D porphyrin organic framework (POF) on 2D graphene and converting the surface POF layer into a pyrrolic-/pyridinic-nitrogen (prN-/pnN)-enriched skin through subsequent pyrolysis aiming at achieving super electrical conductivity and strong LiPS chemisorptivity. Through this design, the graphene backbone without the electronic interference from heteroatoms serves as an electron expressway to expedite electron transfer, while the fully exposed nitrogen species (prN/pnN) with well-certified lithiophilicity maximize the chemisorptive effect to LiPSs, restricting their diffusion. As a result, PNG with spatially modulated dopant distribution exhibits as a much more superior sulfur host than undoped graphene with poor affinity to LiPSs and homogeneously nitrogen-doped graphene (NG) that suffers from low electrical conductivity (Figure 1). According to such a demonstration, a key yet usually underappreciated aspect is revealed: if the electron and LiPS transports are regulated rationally throughout a single material design, the previously suggested trade-off between strong LiPS chemisorption and high electronic conductivity for a sulfur host material can be circumvented. The proposed concept of spatially modulated doping is responsible to the high immobilization efficiency of LiPSs and effective electrocatalysis of sulfur-speciation improvement of Li-S batteries.

To fabricate the PNG host, a POF layer was first deposited on 2D graphene substrate as a conformal and thin coating (referred to G@POF) and then was pyrolyzed into a pyrrolic-/pyridinic-nitrogen-enriched skin decorating the pristine hydrophobic graphene (Figure 2a). In this material design, graphene not only remains as the highly conductive internal backbone of PNG, but also serves as a 2D template to aid the conformal growth of POF. Attributed to the extremely huge conjugated system of graphene, aromatic precursors of POF, such as benzene-1,4-dicarboxaldehyde and pyrrole, can be easily adsorbed on the surface of graphene rather than self-packed, driven by strong π - π interactions. Therefore, a thin and conformal 2D coating of POF was obtained, in which each porphyrin unit was covalently connected by rigid benzene linkers to form a steady framework. The successful hybridization of POF with graphene substrate is evidenced by the intense diffraction peak at $2\theta = 13^\circ$, which is assigned as the intrinsic signal of POF with ordered structure (Figure S1a, Supporting Information). The D-band to G-band (I_D/I_G) ratio of G@POF was 1.121, which is higher than pristine graphene (0.949) (Figure S1b, Supporting Information). The marked increase in I_D/I_G ratio also conforms to the presence of polar POF on the graphene. Such a unique structure is presumably recognized as the origin for the high maintenance of prN/pnN species after pyrolysis at 950 °C for

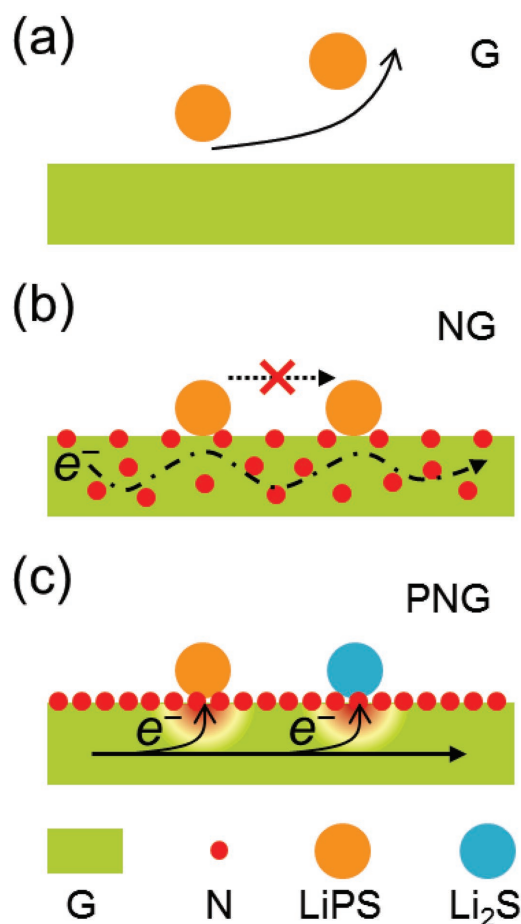


Figure 1. Schematic illustration of key roles of PNG for sulfur species. Conversional graphene (G) with nonpolar nature exhibits poor affinity to LiPSs. Nitrogen-doped graphene favors LiPS affinity but is limited by low electronic conductivity. PNG allows to simultaneously mediate electron and LiPS transport to the efficient operation of Li-S batteries.

6.0 h. The morphology evolution during the fabrication of PNG is indistinguishable (Figure S2a–c, Supporting Information), suggesting that 1) the desirable 2D morphology of graphene was preserved, favoring large atomic exposure; 2) there is no noticeable POF aggregation; 3) the thickness of external prN-/pnN-enriched skin should be very thin to render indiscernible changes in the contrast of electron microscopic images.

In addition, the deposition of POF on graphene and its conversion to the external skin were further confirmed by probing the changes in atomic nitrogen content determined by X-ray photoelectron spectroscopy (XPS) (Figure 2b). Pristine graphene possesses a negligible nitrogen content, which increases to 3.66% for G@POF and then is cut by nearly a half to 1.71% for the pyrolyzed product PNG (inset in Figure 2b). Energy-dispersive spectrometric mapping confirms the uniform nitrogen distribution on the surface of PNG (Figure S3, Supporting Information). Well-fitted N 1s fine scan XPS spectrum of PNG further suggests the dominated nitrogen species of prN (400.1 eV) and pnN (398.7 eV) along with a small amount of quaternary N (qN, 401.1 eV) (inset in Figure 2b).^[30] The dominance of prN and pnN plays a key role in enabling strong lithium bonds to

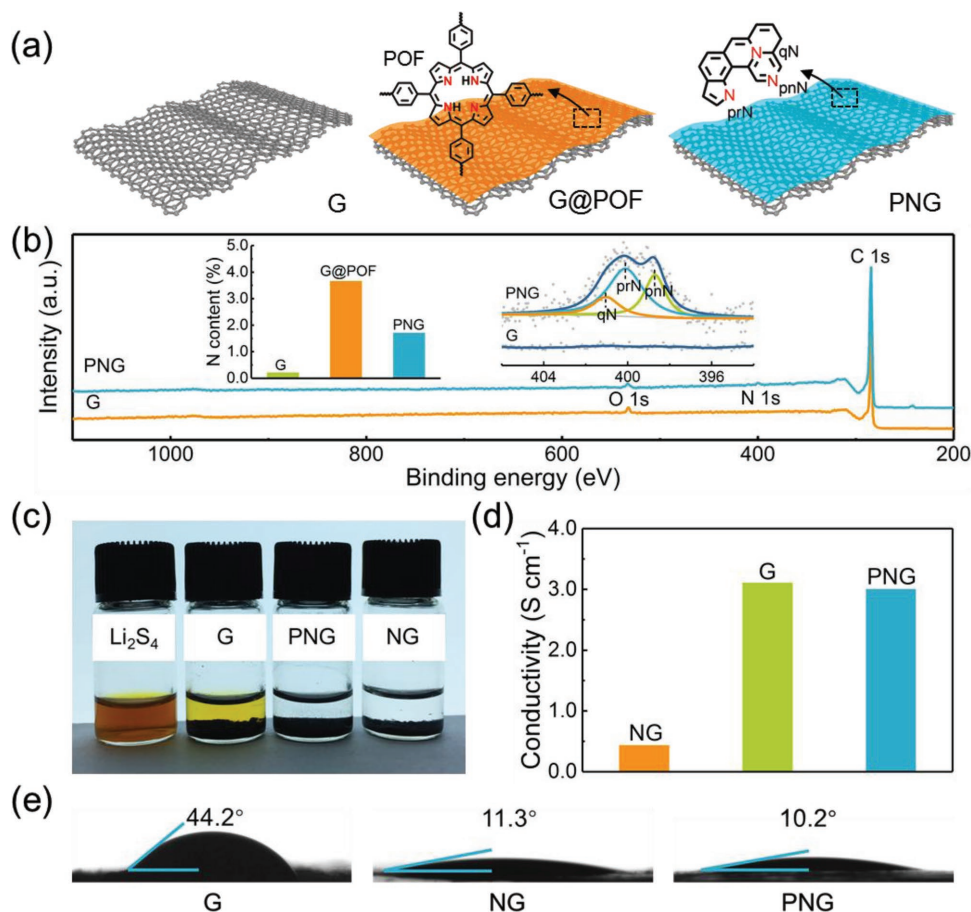


Figure 2. Preparation and characterization of PNG. a) PNG was prepared by conformally growing POF on G and then subjected to pyrolysis. b) XPS analysis for G and PNG (insets are fitting result of the N 1s fine scan XPS spectra to probe nitrogen species and nitrogen content in different materials measured by XPS). c) Static adsorption of Li_2S_4 by various adsorbents after 24 h. d) Electronic conductivities and e) contact angles between electrolyte and different graphene derivations.

trap LiPSs, whereas qN is less efficient in binding LiPSs.^[13] Although the Brunauer-Emmett-Teller (BET) surface areas of G ($602 \text{ m}^2 \text{ g}^{-1}$), NG ($544 \text{ m}^2 \text{ g}^{-1}$), and PNG ($572 \text{ m}^2 \text{ g}^{-1}$) exhibit similar values, the surface-enriched anchoring sites of prN/pnN, in combination with abundant pores (Figure S4, Supporting Information), render PNG a superior sulfur host with an extraordinary specific chemisorption amount for LiPSs as PNG decolorized the LiPS solution thoroughly, while graphene did not (Figure 2c). The accurate surface chemistry was further examined by collecting XPS spectra of PNG before and after LiPS adsorption (Figure S5, Supporting Information). The N 1s and Li 1s XPS spectra exhibit a redshift and a blueshift of characteristic peaks, respectively, both corresponding to the emergence of Li–N interactions as lithium-bond chemistry validated.^[13]

The electrical conductivity of bulk materials is another key parameter of equal importance to LiPS chemisorption. As validated in LiPS adsorption experiment, NG made through a conventional synthetic route (see Supporting Information) also exhibits superior capability of decoloring the LiPS solution and therefore strong chemisorptivity to LiPSs (Figure 2c). Nevertheless, measured by the four-probe method, the electrical conductivity of NG (0.43 S cm^{-1}) is lowered by nearly an order of

magnitude than pristine graphene (3.10 S cm^{-1}) (Figure 2d). On the contrary, PNG exhibits a comparable electrical conductivity (3.00 S cm^{-1}) to graphene, and therefore the superiority of as-demonstrated synthetic strategy in concurrently regulating the electron and LiPS transports is validated. Such superiority is further reflected by enhanced electrolyte wettability of PNG, to which the microscopic redox kinetics are usually correlated as a macroscopic indicator (Figure 2e).^[12] Accordingly, the PNG possesses all-around superiorities regarding LiPS affinity, electrical conductivity, and electrolyte wettability over graphene or NG.

The excellent electrical conductivity and precisely modulated surface chemistry synergistically endows PNG a superb ability to manipulate rapid sulfur conversion reactions. Both electrochemical impedance spectra (EIS) and cyclic voltammetry (CV) were performed in symmetric cells employing two identical graphene-, NG-, or PNG-coated aluminum foil electrodes and a $0.50 \text{ M Li}_2\text{S}_6$ electrolyte. The symmetric cell precludes the interferences from lithium metal anode ubiquitously occurring in the asymmetric Li–S cell configuration, allowing us to investigate the exact redox kinetics at desired interfaces.^[6,20] The NG electrode displays exceptionally huge charge-transfer impedance than graphene and PNG due to its low electrical conductivity (Figure 3a). Graphene, though manifesting rapid electron

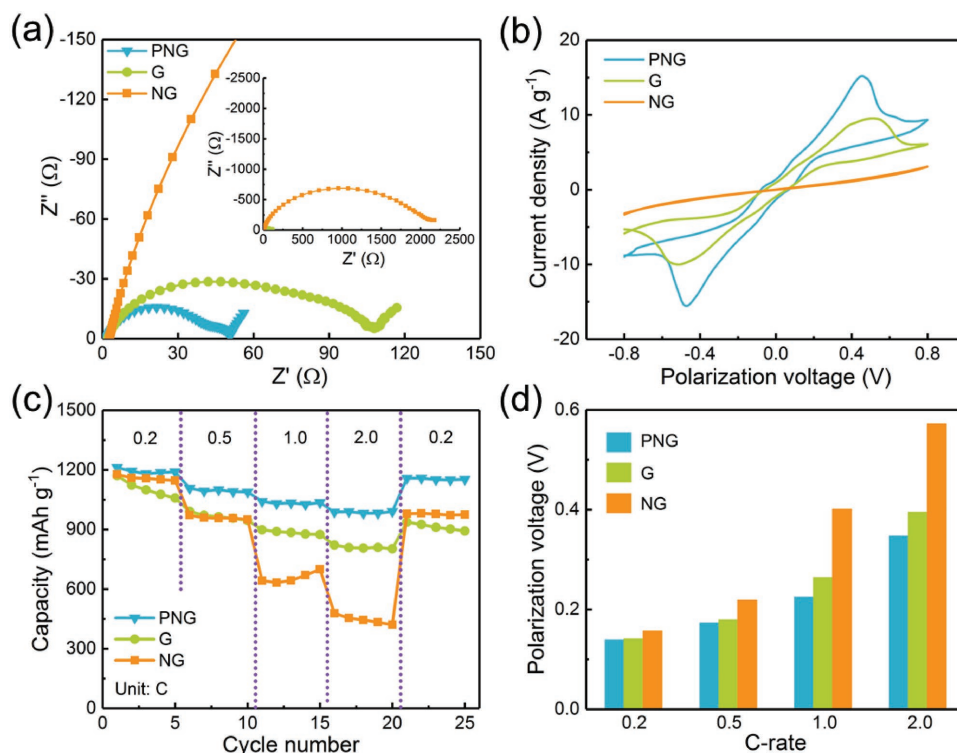


Figure 3. Rapid redox kinetics of PNG. a) EIS and b) CV of symmetric cells of G, NG, and PNG electrodes with Li_2S_6 electrolyte (inset in panel (a) is the full view of EIS). c) Rate capability of Li-S cells and d) overpotential evolution of cells with different current densities.

transfer through its bulk phase, possesses a larger impedance than PNG, which is rationalized by the fact that enhanced LiPS affinity and electrolyte wettability of PNG benefit the access to LiPSs and thus assist rapid charge transfer across the PNG/electrolyte interface. Similarly, CV curves elucidate the same trend: NG exhibits almost linear resistance behavior without any redox peak in the applied potential window, corresponding to a slow redox kinetics; on graphene, phase evolution reactions (i.e., liquid LiPSs to solid sulfur or $\text{Li}_2\text{S}_2/\text{Li}_2\text{S}$) indeed take place as there are noticeable redox peaks corresponding to transport limitations, namely the generation of immobile phases, but these peaks are generally broad and with large polarizations (-0.53 and 0.51 V for cathodic and anodic, respectively), indicating a moderate redox kinetics; only PNG displays the sharpest and most intensive redox peaks, along with relatively small polarizations (-0.47 and 0.45 V for cathodic and anodic, respectively), demonstrating the most expeditious kinetics feature (Figure 3b). The kinetics study performed on symmetric cells unambiguously proves the indispensable role of both LiPS affinity and electrical conductivity in determining the reaction behaviors of sulfur cathode in Li-S batteries.

When demonstrated in actual Li-S cells, PNG was infiltrated on polypropylene separators with an areal mass loading of 0.11 mg cm^{-2} to serve as a lightweight functional interlayer. The inactive mass was not increased significantly. The cell with a PNG interlayer delivers an initial discharge capacity of 1212 mAh g^{-1} at 0.2 C ($1 \text{ C} = 1675 \text{ mA g}^{-1}$) (Figure 3c). Further increasing the current density to 0.5 , 1.0 , and 2.0 C leads to discharge capacities of 1108 , 1041 , and 988 mAh g^{-1} , respectively. Such a superior rate capability endowed by the PNG interlayer

outperforms controlled cells using a graphene- or NG-coated separator. Owing to the poor interfacial charge transfer between LiPS and graphene, as well as the rapid LiPS leakage from cathode to electrolyte that increased the electrolyte viscosity and thus resistance of lithium-ion transport, the cell with a graphene-coated separator delivers a comparable initial capacity of 1171 mAh g^{-1} at 0.2 C but suffered from relatively fast capacity decay, both upon cycling at the same rate (i.e., 0.2 C) and being operated at increasing current densities. Unlike graphene, the introduction of NG benefited the stabilization of capacities at a low current density of 0.2 C , suggesting the effect of nitrogen doping in trapping LiPSs. Nevertheless, the cell with an NG interlayer exhibited drastic capacity decay when the current densities are increased stepwise to 0.5 , 1.0 , and 2.0 C . And the capacity at 2.0 C is only half that of the PNG-modified cell (479 mAh g^{-1}). The poorer rate performance of the NG-modified cell than those with a graphene or PNG separator was ascribed to the much lower electrical conductivity of NG. Correspondingly, the polarization voltages at various current rates agree exactly well with the rate capability (Figure 3d). PNG, with both desirable interfacial and bulk charge transfer, enabled the smallest polarization voltage.

One of the decisive roles of PNG is to retard LiPS shuttle such that stable cyclability is expected (Figure 4). Once LiPSs are produced in the working cell, the PNG interlayer is capable of absorbing and blocking LiPS, which is confirmed by fully coverage of sulfur on the thin PNG wall (Figure S6, Supporting Information) after ten cycles. The PNG-modified cell displays an initial capacity of 1135 mAh g^{-1} at 0.5 C and achieved high reversible capacity of 798 mAh g^{-1} after 300 cycles,

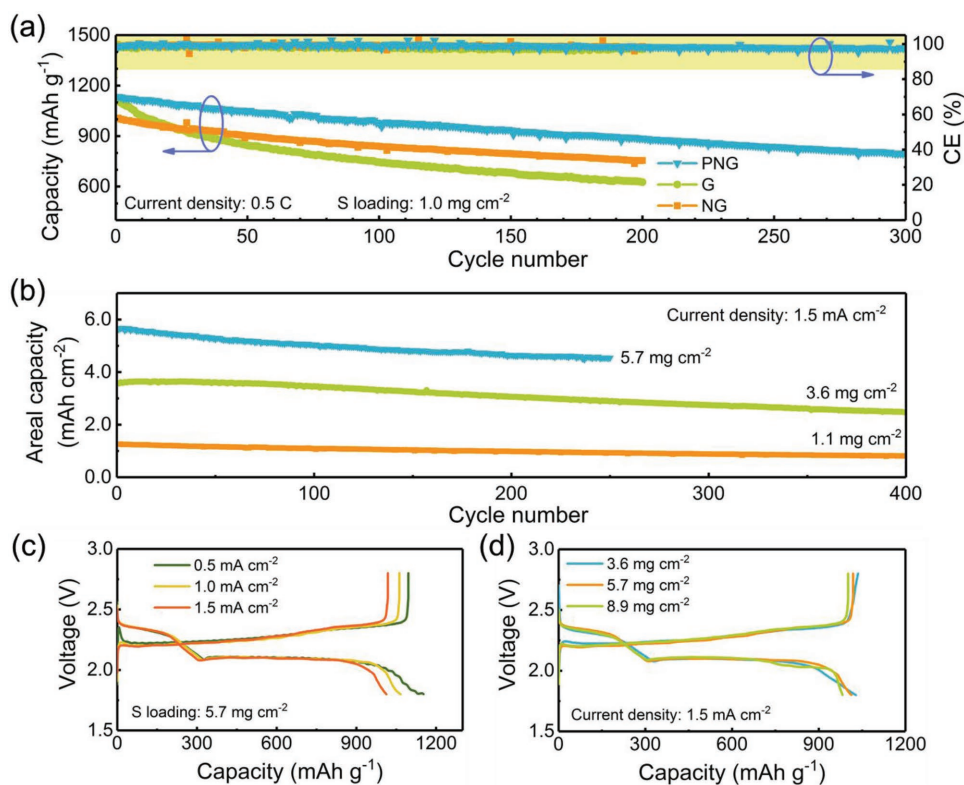


Figure 4. Stable operation of Li-S cells. a) Long-term cycling performance at a current density of 0.5 C. b) Operation of Li-S cells with different S loadings ranging from 1.1 to 5.7 mg cm⁻². c) Galvanostatic discharge-charge profiles of Li-S cell with an S loading of 5.7 mg cm⁻². d) Galvanostatic discharge-charge profiles of Li-S cell with various S loading at a current density of 1.5 mA cm⁻².

corresponding to a cyclic decay rate of 0.099% (Figure 4a). The NG cell exhibits a larger charge transfer resistance than that of the PNG cell, and this tendency is further enlarged after 100 cycles (Figure S7, Supporting Information), indicating superb capability of suppressing LiPS mitigation and facilitating kinetic reactions by PNG. Despite equally impressive capacity of 1106 mAh g⁻¹ in graphene-modified cell, the poor chemisorption of LiPSs by graphene is responsible for rapid capacity decline. Only a capacity of 626 mAh g⁻¹ was preserved after 200 cycles, in accordance with a cyclic decay rate twofold faster than that of PNG-modified cell (0.217%). The strong LiPS affinity of NG endowed the cell with a similar cyclic decay trend to that of PNG-modified one, yet its low electrical conductivity restrained the overall capacity of cell to, for example, 755 mAh g⁻¹ at the 200th cycle. The ultralong cyclability of the Li-S cell enabled by PNG interlayer was also examined at high current densities at 1.0 and 2.0 C, respectively (Figure S8, Supporting Information). Capacities of 613 and 582 mAh g⁻¹ were achieved after 1000 cycles at 1.0 and 2.0 C, corresponding to low cyclic decay rates of 0.042% and 0.040%, respectively. The long-term cyclability at relatively high current densities proves the efficiency of PNG interlayer in trapping LiPSs and facilitating their conversion simultaneously.

To validate the superiority of PNG in more practical conditions, sulfur cathodes with a set of sulfur loadings from 1.1 to 8.9 mg cm⁻² were tested with PNG interlayers at various current densities. The sulfur cathodes with areal sulfur loadings of 1.1 and 3.6 mg cm⁻² exhibited stale cycling with extended

lives, achieving areal capacities of 0.81 and 2.48 mAh cm⁻² after 400 cycles (Figure 4b). The cell with an even higher loading of 5.7 mg cm⁻² maintains an areal capacity of 4.54 mAh cm⁻² after 250 cycles. Even at an ultrahigh loading of 8.9 mg cm⁻², the PNG interlayer enabled the Li-S cell to deliver a very high initial areal capacity of 8.81 mAh cm⁻² and to survive for more than 200 cycles (Figure S9, Supporting Information). Besides the stable cycling performance at high sulfur loadings, the introduction of PNG also ensured reversible operation of thick cathodes at various current densities, which manifested the distinct two-plateau discharge feature with small polarizations and capacities of above 1000 mAh g⁻¹ (>5.7 mAh cm⁻²) at 0.5, 1.0, and 1.5 mA cm⁻² (Figure 4c). At a fixed current density of 1.5 mA cm⁻², the charge-discharge profiles maintained very similar despite different sulfur loadings (Figure 4d). The presented battery performance with high sulfur loadings and at various current densities further evidences kinetic toughness of the proposed concept of designing surface-dopant-enriched and internal conductive host materials like PNG.

In summary, PNG were proposed as advanced sulfur hosts featuring an external nitrogen-enriched atomic layer with strong LiPS affinity and an internal electrically conductive graphene backbone. PNG therefore concurrently favored strong chemisorption to LiPSs and rapid kinetics of sulfur conversion reactions, enabling the operation of working Li-S batteries with high stability, outstanding rate capability, and practically appealing sulfur loadings. Through the rational design of spatially separated LiPS anchoring sites and the conductive

skeleton, PNG circumvented the dilemma of conductive polar sulfur hosts that high dopant number and good bulk electrical conductivity are always in trade-off, thereby exhibiting as much more superb hosts than undoped graphene and homogeneously doped NG. The presented work affords a distinct interfacial strategy to regulate the transport and reaction behaviors of sulfur species and is expected to apply to other conversion reaction batteries relying on dissolution–precipitation mechanism and requiring interfacial charge- and mass-transport-mediation concurrently.

Supporting Information

Supporting Information is available from the Wiley Online Library or from the author.

Acknowledgements

L.K. and B.-Q.L. contributed equally to this work. This work was supported by the National Key Research and Development Program (2016YFA0202500 and 2016YFA0200102), National Natural Science Foundation of China (21776019 and 21676160), and Young Elite Scientists Sponsorship Program by CAST (YESS20150133). The authors thank Xiang Chen and Hong Yuan for their helpful discussions.

Conflict of Interest

The authors declare no conflict of interest.

Keywords

graphene, kinetics, lithium–sulfur batteries, polysulfide, porphyrin

Received: March 15, 2018
Published online: April 19, 2018

- [1] a) J. W. Choi, D. Aurbach, *Nat. Rev. Mater.* **2016**, *1*, 16013; b) A. Manthiram, S. H. Chung, C. Zu, *Adv. Mater.* **2015**, *27*, 1980; c) J. Liang, Z.-H. Sun, F. Li, H.-M. Cheng, *Energy Storage Mater.* **2016**, *2*, 76.
- [2] a) H. J. Peng, J. Q. Huang, X. B. Cheng, Q. Zhang, *Adv. Energy Mater.* **2017**, *7*, 1700260; b) H.-J. Peng, J.-Q. Huang, Q. Zhang, *Chem. Soc. Rev.* **2017**, *46*, 5237; c) Z. W. Seh, Y. Sun, Q. Zhang, Y. Cui, *Chem. Soc. Rev.* **2016**, *45*, 5605.
- [3] L. Borchardt, M. Oschatz, S. Kaskel, *Chem. - Eur. J.* **2016**, *22*, 7324.
- [4] J. Xu, T. Lawson, H. Fan, D. Su, G. Wang, *Adv. Energy Mater.* **2018**, *8*, 1702607.
- [5] a) Q. Pang, X. Liang, C. Y. Kwok, L. F. Nazar, *Nat. Energy* **2016**, *1*, 16132; b) R. Fang, S. Zhao, Z. Sun, D. W. Wang, H. M. Cheng, F. Li, *Adv. Mater.* **2017**, *29*, 1606823.
- [6] G. Zhang, Z. W. Zhang, H. J. Peng, J. Q. Huang, Q. Zhang, *Small Methods* **2017**, *1*, 1700134.
- [7] a) G. Li, Z. Chen, J. Lu, *Chem* **2018**, *4*, 3; b) J. Zhang, H. Huang, J. Bae, S. H. Chung, W. Zhang, A. Manthiram, G. Yu, *Small Methods* **2018**, *2*, 1700279.
- [8] a) Z. Li, H. B. Wu, X. W. D. Lou, *Energy Environ. Sci.* **2016**, *9*, 3061; b) X. Yu, A. Manthiram, *Acc. Chem. Res.* **2017**, *50*, 2653.
- [9] a) Y. Li, J. Fan, J. Zhang, J. Yang, R. Yuan, J. Chang, M. Zheng, Q. Dong, *ACS Nano* **2017**, *11*, 11417; b) K. Mi, S. Chen, B. Xi, S. Kai, Y. Jiang, J. Feng, Y. Qian, S. Xiong, *Adv. Funct. Mater.* **2017**, *27*, 1604265; c) S. H. Chung, A. Manthiram, *Adv. Mater.* **2018**, *30*, 1705951; d) Y. Ye, F. Wu, Y. Liu, T. Zhao, J. Qian, Y. Xing, W. Li, J. Huang, L. Li, Q. Huang, X. Bai, R. Chen, *Adv. Mater.* **2017**, *29*, 1700598; e) Y. Mao, G. Li, Y. Guo, Z. Li, C. Liang, X. Peng, Z. Lin, *Nat. Commun.* **2017**, *8*, 14628; f) C.-W. Lee, Q. Pang, S. Ha, L. Cheng, S.-D. Han, K. R. Zavadil, K. G. Gallagher, L. F. Nazar, M. Balasubramanian, *ACS Cent. Sci.* **2017**, *3*, 605; g) S.-H. Chung, A. Manthiram, *Joule* **2018**, <https://doi.org/10.1016/j.joule.2018.01.002>.
- [10] a) H. J. Peng, W. T. Xu, L. Zhu, D. W. Wang, J. Q. Huang, X. B. Cheng, Z. Yuan, F. Wei, Q. Zhang, *Adv. Funct. Mater.* **2016**, *26*, 6351; b) X. Ji, K. T. Lee, L. F. Nazar, *Nat. Mater.* **2009**, *8*, 500; c) H. J. Peng, J. Q. Huang, M. Q. Zhao, Q. Zhang, X. B. Cheng, X. Y. Liu, W. Z. Qian, F. Wei, *Adv. Funct. Mater.* **2014**, *24*, 2772; d) W. Li, Z. Liang, Z. Lu, H. Yao, Z. W. Seh, K. Yan, G. Zheng, Y. Cui, *Adv. Energy Mater.* **2015**, *5*, 1500211; e) H. Wang, W. Zhang, H. Liu, Z. Guo, *Angew. Chem., Int. Ed.* **2016**, *55*, 3992.
- [11] a) H. J. Peng, Z. W. Zhang, J. Q. Huang, G. Zhang, J. Xie, W. T. Xu, J. L. Shi, X. Chen, X. B. Cheng, Q. Zhang, *Adv. Mater.* **2016**, *28*, 9551; b) X. Liang, C. Hart, Q. Pang, A. Garsuch, T. Weiss, L. F. Nazar, *Nat. Commun.* **2015**, *6*, 5682; c) F. Pei, T. An, J. Zang, X. Zhao, X. Fang, M. Zheng, Q. Dong, N. Zheng, *Adv. Energy Mater.* **2016**, *6*, 1502539.
- [12] a) G. P. Hao, C. Tang, E. Zhang, P. Zhai, J. Yin, W. Zhu, Q. Zhang, S. Kaskel, *Adv. Mater.* **2017**, *29*, 1702829; b) J.-Y. Hwang, H. M. Kim, Y.-K. Sun, *J. Electrochem. Soc.* **2018**, *165*, A5006.
- [13] T.-Z. Hou, W.-T. Xu, X. Chen, H.-J. Peng, J.-Q. Huang, Q. Zhang, *Angew. Chem., Int. Ed.* **2017**, *56*, 8178.
- [14] a) J. Song, M. L. Gordin, T. Xu, S. Chen, Z. Yu, H. Sohn, J. Lu, Y. Ren, Y. Duan, D. Wang, *Angew. Chem. Int. Ed.* **2015**, *54*, 4325; b) Q. Pang, J. Tang, H. Huang, X. Liang, C. Hart, K. C. Tam, L. F. Nazar, *Adv. Mater.* **2015**, *27*, 6021; c) Y. Qiu, W. Li, W. Zhao, G. Li, Y. Hou, M. Liu, L. Zhou, F. Ye, H. Li, Z. Wei, S. Yang, W. Duan, Y. Ye, J. Guo, Y. Zhang, *Nano Lett.* **2014**, *14*, 4821; d) T. Z. Hou, X. Chen, H. J. Peng, J. Q. Huang, B. Q. Li, Q. Zhang, B. Li, *Small* **2016**, *12*, 3283; e) H. Yuan, W. Zhang, J.-g. Wang, G. Zhou, Z. Zhuang, J. Luo, H. Huang, Y. Gan, C. Liang, Y. Xia, J. Zhang, X. Tao, *Energy Storage Mater.* **2018**, *10*, 1.
- [15] B. Guo, Q. Liu, E. Chen, H. Zhu, L. Fang, J. R. Gong, *Nano Lett.* **2010**, *10*, 4975.
- [16] a) Z. Li, B. Y. Guan, J. Zhang, X. W. D. Lou, *Joule* **2017**, *1*, 576; b) X. Liu, J. Q. Huang, Q. Zhang, L. Mai, *Adv. Mater.* **2017**, *29*, 1601759; c) L. Kong, H.-J. Peng, J.-Q. Huang, W. Zhu, G. Zhang, Z.-W. Zhang, P.-Y. Zhai, P. Sun, J. Xie, Q. Zhang, *Energy Storage Mater.* **2017**, *8*, 153; d) X. Wang, G. Li, J. Li, Y. Zhang, A. Wook, A. Yu, Z. Chen, *Energy Environ. Sci.* **2016**, *9*, 2533; e) X. Wang, T. Gao, X. Fan, F. Han, Y. Wu, Z. Zhang, J. Li, C. Wang, *Adv. Funct. Mater.* **2016**, *26*, 7164.
- [17] a) K. Xie, Y. You, K. Yuan, W. Lu, K. Zhang, F. Xu, M. Ye, S. Ke, C. Shen, X. Zeng, X. Fan, B. Wei, *Adv. Mater.* **2017**, *29*, 1604724; b) L. Kong, X. Chen, B. Q. Li, H. J. Peng, J. Q. Huang, J. Xie, Q. Zhang, *Adv. Mater.* **2018**, *30*, 1705219.
- [18] Z. Yuan, H.-J. Peng, T.-Z. Hou, J.-Q. Huang, C.-M. Chen, D.-W. Wang, X.-B. Cheng, F. Wei, Q. Zhang, *Nano Lett.* **2016**, *16*, 519.
- [19] a) C. Ye, L. Zhang, C. Guo, D. Li, A. Vasilieff, H. Wang, S. Z. Qiao, *Adv. Funct. Mater.* **2017**, *27*, 1702524; b) M. Zhang, C. Yu, C. Zhao, X. Song, X. Han, S. Liu, C. Hao, J. Qiu, *Energy Storage Mater.* **2016**, *5*, 223; c) T. Lei, W. Chen, J. Huang, C. Yan, H. Sun, C. Wang, W. Zhang, Y. Li, J. Xiong, *Adv. Energy Mater.* **2017**, *7*, 1601843; d) J. Park, B. C. Yu, J. S. Park, J. W. Choi, C. Kim, Y. E. Sung, J. B. Goodenough, *Adv. Energy Mater.* **2017**, *7*, 1602567; e) S. S. Zhang, *J. Mater. Chem. A* **2015**, *3*, 7689.

- [20] H. J. Peng, G. Zhang, X. Chen, Z. W. Zhang, W. T. Xu, J. Q. Huang, Q. Zhang, *Angew. Chem., Int. Ed.* **2016**, *128*, 12990.
- [21] a) Z. Cui, C. Zu, W. Zhou, A. Manthiram, J. B. Goodenough, *Adv. Mater.* **2016**, *28*, 6926; b) T. Zhou, W. Lv, J. Li, G. Zhou, Y. Zhao, S. Fan, B. Liu, B. Li, F. Kang, Q.-H. Yang, *Energy Environ. Sci.* **2017**, *10*, 1694; c) Z. Sun, J. Zhang, L. Yin, G. Hu, R. Fang, H.-M. Cheng, F. Li, *Nat. Commun.* **2017**, *8*, 14627.
- [22] X. Liang, A. Garsuch, L. F. Nazar, *Angew. Chem., Int. Ed.* **2015**, *54*, 3907.
- [23] H. Yuan, X. Chen, G. Zhou, W. Zhang, J. Luo, H. Huang, Y. Gan, C. Liang, Y. Xia, J. Zhang, *ACS Energy Lett.* **2017**, *2*, 1711.
- [24] a) C. Hu, H. Chen, Y. Shen, D. Lu, Y. Zhao, A.-H. Lu, X. Wu, W. Lu, L. Chen, *Nat. Commun.* **2017**, *8*, 479; b) Y. Liu, W. Wang, A. Wang, Z. Jin, H. Zhao, Y. Yang, *J. Mater. Chem. A* **2017**, *5*, 22120; c) C. Y. Chen, H. J. Peng, T. Z. Hou, P. Y. Zhai, B. Q. Li, C. Tang, W. Zhu, J. Q. Huang, Q. Zhang, *Adv. Mater.* **2017**, *29*, 1606802; d) L. Li, T. A. Pascal, J. G. Connell, F. Y. Fan, S. M. Meckler, L. Ma, Y.-M. Chiang, D. Prendergast, B. A. Helms, *Nat. Commun.* **2017**, *8*, 2277.
- [25] a) J. Zheng, J. Tian, D. Wu, M. Gu, W. Xu, C. Wang, F. Gao, M. H. Engelhard, J.-G. Zhang, J. Liu, J. Xiao, *Nano Lett.* **2014**, *14*, 2345; b) X. Liang, Y. Rangom, C. Y. Kwok, Q. Pang, L. F. Nazar, *Adv. Mater.* **2017**, *29*, 1603040.
- [26] a) X. Tao, J. Wang, Z. Ying, Q. Cai, G. Zheng, Y. Gan, H. Huang, Y. Xia, C. Liang, W. Zhang, Y. Cui, *Nano Lett.* **2014**, *14*, 5288; b) T. Chen, Z. Zhang, B. Cheng, R. Chen, Y. Hu, L. Ma, G. Zhu, J. Liu, Z. Jin, *J. Am. Chem. Soc.* **2017**, *139*, 12710.
- [27] a) H. Lin, L. Yang, X. Jiang, G. Li, T. Zhang, Q. Yao, G. W. Zheng, J. Y. Lee, *Energy Environ. Sci.* **2017**, *10*, 1476; b) H. Al Salem, G. Babu, C. V. Rao, L. M. R. Arava, *J. Am. Chem. Soc.* **2015**, *137*, 11542; c) G. Zhou, H. Tian, Y. Jin, X. Tao, B. Liu, R. Zhang, Z. W. Seh, D. Zhuo, Y. Liu, J. Sun, J. Zhao, C. Zu, D. S. Wu, Q. Zhang, Y. Cui, *Proc. Natl. Acad. Sci. USA* **2017**, *114*, 840; d) L. Li, L. Chen, S. Mukherjee, J. Gao, H. Sun, Z. Liu, X. Ma, T. Gupta, C. V. Singh, W. Ren, H.-M. Cheng, N. Koratkar, *Adv. Mater.* **2017**, *29*, 1602734.
- [28] a) X. Tao, J. Wang, C. Liu, H. Wang, H. Yao, G. Zheng, Z. W. Seh, Q. Cai, W. Li, G. Zhou, C. Zu, Y. Cui, *Nat. Commun.* **2016**, *7*, 11203; b) X. Liu, N. Xu, T. Qian, J. Liu, X. Shen, C. Yan, *Small* **2017**, *13*, 1702104.
- [29] a) Z. Zhang, L. L. Kong, S. Liu, G. R. Li, X. P. Gao, *Adv. Energy Mater.* **2017**, *7*, 1602543; b) D. Su, M. Cortie, H. Fan, G. Wang, *Adv. Mater.* **2017**, *29*, 1700587; c) T. Zhao, Y. Ye, X. Peng, G. Divitini, H. K. Kim, C. Y. Lao, P. R. Coxon, K. Xi, Y. Liu, C. Ducati, R. Chen, R. V. Kumar, *Adv. Funct. Mater.* **2016**, *26*, 8418; d) Y. Lai, P. Wang, F. Qin, M. Xu, J. Li, K. Zhang, Z. Zhang, *Energy Storage Mater.* **2017**, *9*, 179.
- [30] H. Wang, T. Maiyalagan, X. Wang, *ACS Catal.* **2012**, *2*, 781.